Enhanced Omnidirectional Photovoltaic Performance of Solar Cells Using Multiple-Discrete-Layer Tailored- and Low-Refractive Index Anti-Reflection Coatings

*Xing Yan, David J. Poxson, Jaehee Cho, Roger E. Welser, Ashok K. Sood, Jong Kyu Kim, and E. Fred Schubert**

An optimized four-layer tailored- and low-refractive index anti-reflection (AR) coating on an inverted metamorphic (IMM) triple-junction solar cell device is demonstrated. Due to an excellent refractive index matching with the ambient air by using tailored- and low-refractive index nanoporous SiO_2 layers and owing to a multiple-discrete-layer design of the AR coating optimized by a genetic algorithm, such a four-layer AR coating shows excellent broadband and omnidirectional AR characteristics and significantly enhances the omnidirectional photovoltaic performance of IMM solar cell devices. Comparing the photovoltaic performance of an IMM solar cell device with the four-layer AR coating and an IMM solar cell with the conventional SiO_2/TiO_2 double layer AR coating, the four-layer AR coating achieves an angle-of-incidence (AOI) averaged short-circuit current density, J_{SC}, enhancement of 34.4%, whereas the conventional double layer AR coating only achieves an AOI-averaged J_{SC} enhancement of 25.3%. The measured reflectance reduction and omnidirectional photovoltaic performance enhancement of the four-layer AR coating are to our knowledge, the largest ever reported in the literature of solar cell devices.

1. Introduction

Photovoltaic (PV) energy is becoming an attractive source of renewable energy owing to the abundance of solar energy on the planet earth, the minimal environmental impact of photovoltaic energy conversion, and the ever-advancing power conversion efficiency of PV technologies.[1] An important and well known phenomenon lowering the overall power conversion efficiency of solar cell devices is Fresnel reflection, occurring when a refractive index contrast exists between the ambient medium (air) and the solar cell device (semiconductor). Anti-reflection (AR) coatings are an indispensable component to reduce or suppress Fresnel reflection losses, to increase the amount of light entering the PV device and hence, to enhance the power conversion efficiency of solar cells. Recently, through better utilization of the solar spectrum, solar cells with a multijunction design have achieved over 40% power conversion efficiency.[2] As PV technologies continue to improve, the demand for better AR coatings also increases.

Traditionally, single layer quarter-wavelength coatings and double layer AR (DLAR) coatings have been used to reduce Fresnel reflective losses.[3–7] However, these conventional AR coatings offer effective AR performance only over a narrow band of wavelengths and a narrow range of incident angles. Such constraints of conventional AR coatings are particularly problematic for solar cell applications, for several reasons: First, the solar spectrum is an inherently broadband spectrum; a significant portion of solar spectrum lies outside the optimal AR band of traditional AR coatings. Second, because of the positional variation of the sun throughout the day and year, and because roughly 15% of the solar energy is incident at all angles-of-incidence (AOIs) as diffuse light scattered by the Earth's atmosphere,[8] a significant amount of the solar energy incident on the surface of a solar cell is outside the range of AOIs that traditional AR coatings are optimized for. Third, solar cells for use in concentrator photovoltaic systems with maximum concentration ratio receive concentrated rays impinging on the device surface at incident angles up to $\theta = \pi/2$.[9] Thus,

X. Yan
Department of Physics, Applied Physics and Astronomy, Rensselaer Polytechnic Institute
110 Eighth Street, Troy, NY 12180, USA
Dr. J. Cho, Prof. E. F. Schubert
Department of Electrical Computer, and Systems Engineering
Rensselaer Polytechnic Institute
110 Eighth Street, Troy, NY 12180, USA
E-mail: EFSchubert@rpi.edu
Dr. D. J. Poxson
Rensselaer Nanotechnology Center
Rensselaer Polytechnic Institute
110 Eighth Street, Troy, NY 12180, USA
Dr. R. E. Welser, Dr. A. K. Sood
Magnolia Solar, Inc., 54 Cummings Park
Woburn, MA 01801, USA
Prof. J. K. Kim
Department of Materials Science and Engineering
Pohang University of Science and Technology
Pohang, 790-784, Korea

DOI: 10.1002/adfm.201201032

© 2013 WILEY-VCH Verlag GmbH & Co. KGaA, Weinheim

AR coatings that embody both broadband and omnidirectional AR characteristics are very desirable.

Driven by the demand for AR coatings with better AR characteristics, a variety of alternative AR coating designs have been proposed or demonstrated. Nevertheless, attempts to improve the conventional DLAR coating design using classical coating materials have proved to be challenging.[10] Thus, to further reduce Fresnel reflection losses, novel AR coatings utilizing low-refractive index thin film materials have been studied.[11,12] Technologies relying on the phase separation in a macromolecular liquid[11] or spun-on sol-gel processes,[12] currently suffer from the lack of thin-film thickness and refractive-index control. Yet such control is necessary in the fabrication of high performance optical coatings.

Other encouraging AR-coating technologies are based on subwavelength structures (SWSs)[13–18] inspired by the idea of a continuously graded-refractive index profile, first envisioned by Lord Rayleigh.[19] Some SWSs employ a "top-down" patterning and etching process. Top-down biomimetic "moth-eye" structures can be patterned (disorderly) by self-assembly of nanoparticles,[13,14] or (orderly) by nanoimprint lithography.[15,16] An alternative approach to form SWSs is "bottom-up" growth of tapered nanorods.[17,18] All of these SWSs were reported to strongly suppress broadband and omnidirectional reflectance in typical Si, AlInP/GaAs or GaAs solar cells.[13–18]

In 2005, a new class of tailored- and low-refractive index nanoporous dielectric thin films, fabricated utilizing oblique-angle electron beam (e-beam) deposition methodology, was reported. Such deposition methodology exhibits excellent control over the refractive index and film thickness, while achieving some of the lowest refractive indices ever reported, e.g., n = 1.05.[20,21] These unique and highly desirable optical properties, namely tailored- and low-refractive indices, have been investigated for use in a variety of optical coating applications such as ODRs,[22,23] AR coatings,[24–27] DBRs,[28,29] and optical filters.[30] By incorporating tailored- and low-refractive index materials into AR coating design and fabrication, significant progress[24,25] was made in the implementation of quasi-continuously-graded refractive index AR coatings with so called quintic or modified-quintic profiles.[31] AR coatings with these refractive index profiles are able to achieve better broadband and omnidirectional AR characteristics than conventional DLAR coatings.

More recently, it has been suggested that by utilizing the tailored- and low-refractive index nanoporous materials, AR coatings incorporating a multiple-discrete-layer design with specific optimized refractive index and thickness configurations are capable of better broadband and omnidirectional AR characteristics than quarter-wavelength, DLAR, and even continuously graded-refractive index AR coatings.[32,33] Such multiple-discrete-layer AR coatings make beneficial use of optical interference effects occurring at the interface of AR coating/ambient and AR coating/substrate, where an unavoidable refractive index contrast exists in any real structure.[34,35] Through careful optimization of optical interference effects and fabrication techniques utilizing tailored- and low-refractive index materials, multiple-discrete-layer AR coatings are expected to offer the broadest spectral band and lowest omnidirectional reflectance of any AR coating to date.

In this study, we report on the design and fabrication of a genetic algorithm (GA) optimized four-layer discrete-refractive index AR coating utilizing tailored- and low-refractive index nanoporous thin films (referred to as four-layer ARC) on an inverted metamorphic (IMM) triple-junction solar cell. By combining the unique tailored- and low-refractive index property of the nanoporous thin films and the global optimization of interference AR effects in the AR coating/IMM solar cell structure enabled by a genetic algorithm, we demonstrate the viability and excellent performance of multiple-discrete-layer AR coatings, not only by reflectance measurements, but also by directly measuring the PV device-efficiency enhancement. Additionally, to demonstrate the potential of multiple-discrete-layer AR coating as a superseding technology to the traditional DLAR coating for solar cell industry, we perform a comparative study of theoretical and experimental AR characteristics for the four-layer ARC and a GA-optimized SiO_2/TiO_2 DLAR coating (referred to as DLAR coating). Theory and experiment are found to be in good agreement, indicating that four-layer ARC has substantially improved broadband and omnidirectional AR performance over that of the traditional DLAR coating for applications in IMM solar cell devices.

2. Results and Discussion

The IMM solar cell device,[36] with the four-layer ARC, is schematically shown in **Figure 1**a. The three subcells of the triple-junction solar cell from top to bottom are, in order, the GaInP, GaAs, and GaInAs subcell, designed to work for short, intermediate, and long wavelengths of the solar spectrum, respectively. The four-layer ARC is directly applied to the top AlInP window layer covering the contact grid, as a purely additive component. Both DLAR coating and four-layer ARC structures were each designed using a computational GA optimization methodology[32] (further details of the GA optimization are discussed in the Supporting Information).

Using a fitness function, the GA iteratively searches for the "fittest individuals" (AR coating structures), among a population of randomly generated AR coating structures. At the end of each generation (iteration), a small percentage of the population, which are "individuals" with the lowest fitness values, are discarded. The population is then replenished with new individuals reproduced by crossover and mutation of the non-discarded (cloned) "individuals". The fitness value (F) chosen here, and applied to each AR coating structure, is

$$F = 1 - \langle R(\lambda, \theta) \rangle \quad (1)$$

where $\langle R(\lambda, \theta) \rangle$ is the wavelength-, AOI-, and TE/TM-averaged reflectance of the AR coating. For the calculation of $\langle R(\lambda, \theta) \rangle$, reflectance values at different AOIs that range from 0° to 80° are equally weighted (at each wavelength in the range 350–1600 nm). However, because the IMM solar cells used in this study show a current limiting behavior by the GaInP top subcell, as a tunable optimization parameter of the GA, the weighting of the reflectance values at shorter wavelengths (350–700 nm) was chosen to be four times larger than the weighting of reflectance values at longer wavelengths (700–1600 nm). This wavelength weighting is used only in the process of AR coating design.

© 2013 WILEY-VCH Verlag GmbH & Co. KGaA, Weinheim

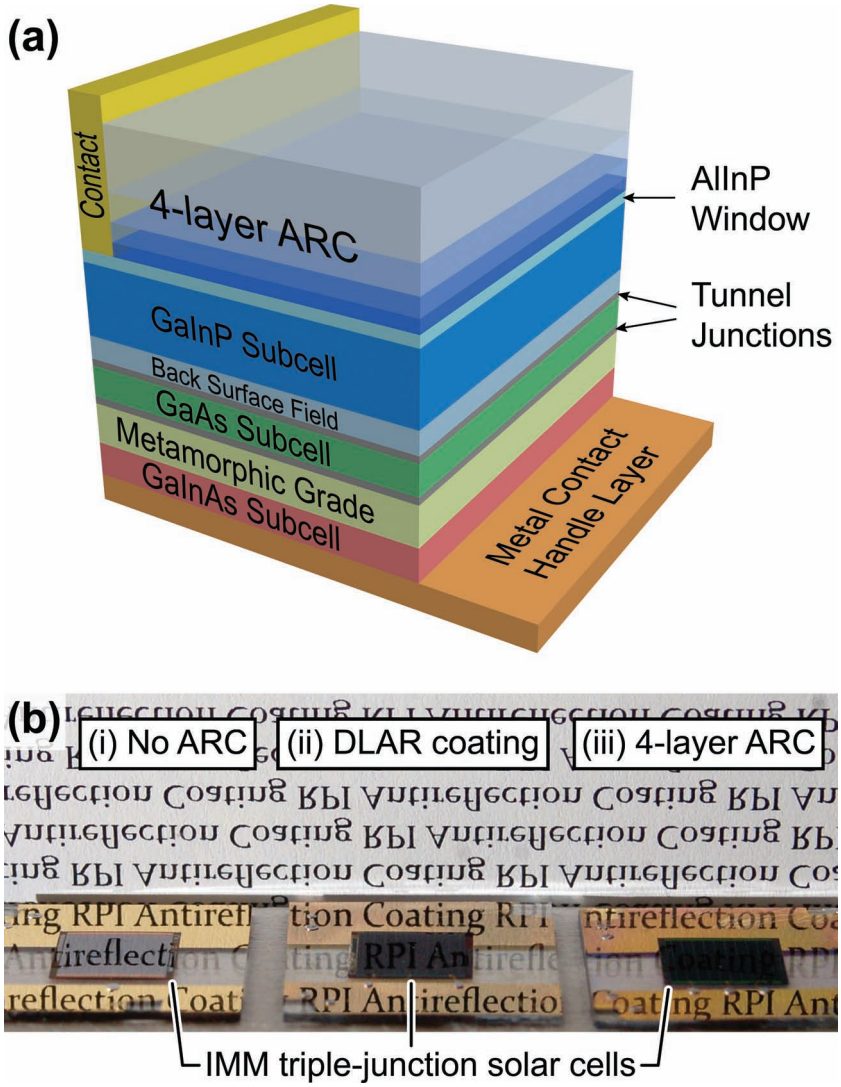

Figure 1. a) Schematic layer sequence of an inverted metamorphic (IMM) triple-junction solar cell with four-layer ARC. b) Photograph of three IMM solar cells with (i) no ARC, (ii) DLAR coating, and (iii) four-layer ARC.

The IMM solar cell device model was simplified to be an AlInP window layer (30 nm) on top of a GaInP layer of infinite thickness (both layers are lattice matched to GaAs). Such a simplification was made because the exact IMM device structure is proprietary. However, sample calculations suggest that simplifying the IMM AlInP/GaInP/GaAs/metamorphic grade/GaInAs device structure into an AlInP/GaInP device structure is justified and does not significantly impact the optimized four-layer ARC structure or AR performance of the structure.

For GA-optimization of four-layer ARC, the refractive index for each layer was chosen to be freely tailorable from n = 1.09 (80% nanoporous SiO_2) to n = 2.5 (dense TiO_2); whereas for GA-optimization of the DLAR coating, the layer materials were restricted to be SiO_2 (dense)/TiO_2 (dense). Layer thicknesses for both GA-optimizations of DLAR coating and four-layer ARC are unrestricted. The resulting GA-optimized DLAR coating and four-layer ARC are shown in **Table 1**.

Utilizing oblique-angle e-beam deposition and physical vapor deposition (sputtering) methodology, the GA-optimized DLAR coating and four-layer ARC were each fabricated on an IMM solar cell device. Detailed information on this process can be found in the Experimental section. The completed structure of a four-layer ARC on a Si substrate is shown in the scanning-electron microscopy (SEM) image of **Figure 2**a. From this cross-sectional SEM image, the distinct layer boundaries can readily be identified. The refractive index and thickness of each layer are given in Table 1. As described above,

Table 1. GA-optimized and measured structures (refractive index and thickness) for each layer of the DLAR coating and four-layer ARC.[a,b]

		Refractive index n		Thickness [nm]	
	Deposition method	Measured	GA-optimized	Measured	GA-optimized
DLAR coating					
TiO_2 layer	TiO_2 sputtering	2.38	2.41	44	45
SiO_2 layer	SiO_2 sputtering	1.47	1.46	104	102
Four-layer ARC					
Layer-1	TiO_2 sputtering	2.38	2.41	49	46
Layer-2	SiO_2/TiO_2 co-sputtering	1.79	1.77	77	80
Layer-3	SiO_2 (deposition angle 57°)	1.32	1.34	118	119
Layer-4	SiO_2 (deposition angle 85°)	1.11	1.09	262	225

[a]GA-optimized and measured refractive index obtained at wavelength λ = 500 nm; [b]The measured refractive indices and thicknesses are obtained on Si reference samples.

© 2013 WILEY-VCH Verlag GmbH & Co. KGaA, Weinheim

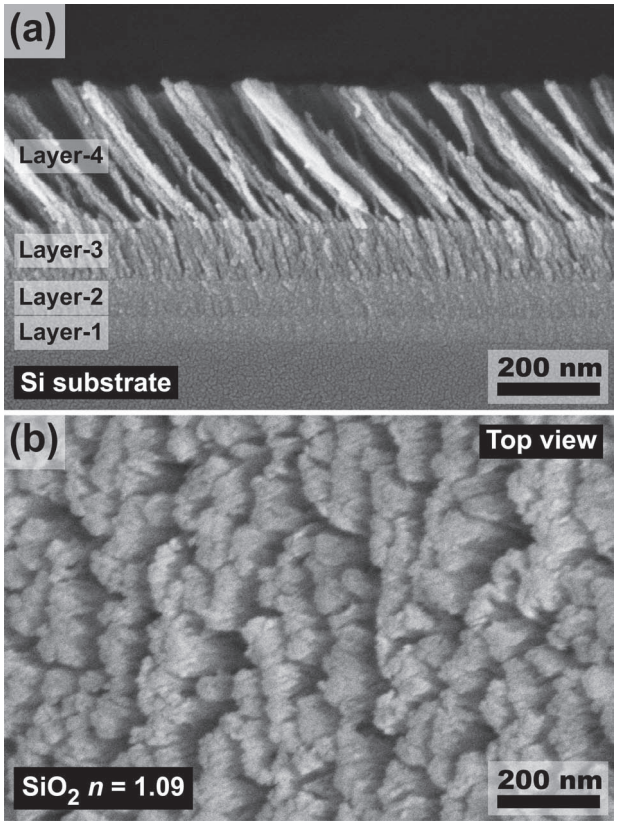

Figure 2. a) SEM cross-sectional image of the four-layer ARC deposited on a Si substrate. Refractive index and thickness information of individual layers are provided in Table 1. b) Top-view SEM image of the nanoporous surface of the four-layer ARC structure.

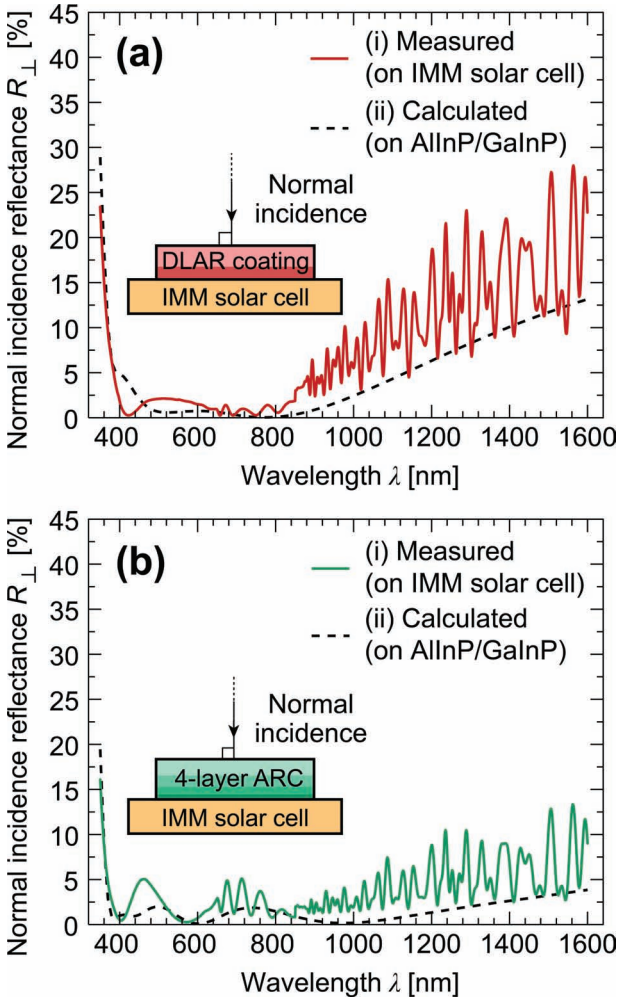

Figure 3. (i) Measured and (ii) calculated normal incidence specular reflectance $R_\perp$ for (a) conventional DLAR coating and (b) four-layer ARC. The measured $R_\perp$ was obtained on IMM solar cells, and the calculated $R_\perp$ was obtained on an AlInP (30 nm)/GaInP (infinitely thick) simplified structure of the IMM solar cell.

oblique-angle deposition shows good control over the thin film nanoporosity (refractive index) and thickness,[37] resulting in good agreement between the AR coating design parameters and actual parameters. We note that the Layer-4 actual thickness of the four-layer ARC has a small deviation from the design thickness. Figure 2b shows a top-view SEM image of the four-layer ARC on a Si substrate. According to this image, the feature length of the nanostructure (e.g., diameter of the nano-rod) is much smaller than the wavelengths of visible light.

Normal incidence specular reflectance is widely used when evaluating the performance of AR coatings. As such, we measured the wavelength-resolved normal incidence specular reflectance for the wavelength range 350–1600 nm for IMM devices coated with either the DLAR coating or the four-layer ARC, and then compared these experimental reflectance values to the calculated TE/TM-averaged normal-incidence reflectance values (see **Figure 3**). It should be noted that the specular reflectance measurements do not account for diffuse reflections (e.g., caused by scattering). However, due to the small feature size of the nanoporous thin films, such scattering losses are often considered to be negligible.[21] Inspection of the figure reveals that the measured reflectances for both the DLAR coating and the four-layer ARC are in good agreement with the calculations. The measured wavelength-averaged normal incidence reflectance is 7.9% for the DLAR coating and 3.9% for the four-layer ARC. The calculated wavelength-averaged normal-incidence reflectance is 4.8% for the DLAR coating and 1.5% for the four-layer ARC. The slightly higher measured reflectance values, as compared to the calculation, probably have occurred because of (i) small differences between refractive index values of the AlInP/GaInP structure used in GA-optimization and those of the actual IMM solar cell devices, and (ii) reflectance off the electrical contact grid on the surface of the IMM devices. The oscillating reflectance spikes shown in the experimental reflectance measurements of both DLAR coating and four-layer ARC are likely caused by the optical interference between the GaInP, GaAs, and GaInAs subcells. From these measurements, and as clearly shown in Figure 3a,b, the four-layer ARC shows remarkably enhanced broadband AR performance over that of the conventional DLAR coating, particularly for near ultraviolet (350–400 nm) and near infrared (850–1600 nm) wavelengths.

While normal incidence total (specular and diffusive) reflectance is an important figure-of-merit of virtually every AR

© 2013 WILEY-VCH Verlag GmbH & Co. KGaA, Weinheim

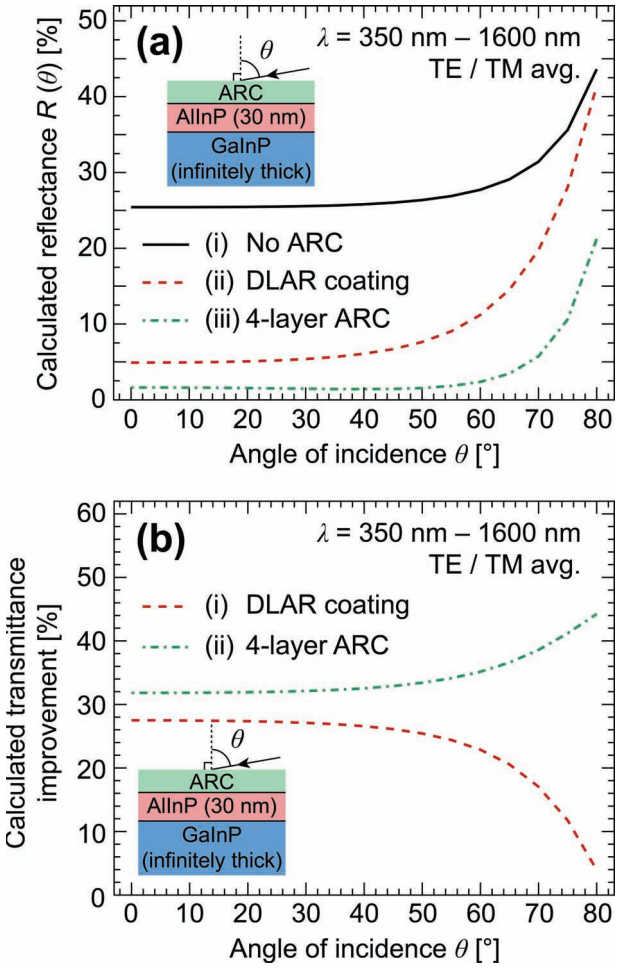

Figure 4. a) Calculated wavelength- and TE/TM-averaged reflectance $R(\theta)$ for AlInP/GaInP structure with (i) no ARC, (ii) DLAR coating, and (iii) four-layer ARC. The AOI-dependent reflectance $R(\theta)$ are equally weighted for the TE and TM mode, and over $\lambda = 350$–1600 nm. b) Calculated transmittance $T(\theta)$ improvement due to (i) DLAR coating and (ii) four-layer ARC. $T(\theta) = 1 - R(\theta)$, assuming no scattering or absorption losses.

coating, the omnidirectional AR performance, which we now show, also plays an important role in solar cell applications. **Figure 4**a plots the calculated wavelength- and TE/TM-averaged reflectance $R(\theta)$. From these calculations, the four-layer ARC shows significantly lower reflectance over all AOIs (0°–80°) than the DLAR coating. The calculated reflectance shown in Figure 4a averaged over all AOIs is 10.1% for the DLAR coating and reduces to 3.1% for the four-layer ARC. This to the best of our knowledge, is the lowest calculated reflectance ever reported for an AR coating on an AlInP/GaInP substrate over this broad range of angles and wavelengths. Figure S3 (Supporting Information) shows a complete evaluation of wavelength- and AOI-dependent reflectance $R(\lambda,\theta)$ for DLAR coating and four-layer ARC.

Figure 4b shows the transmittance $T(\theta)$ improvement of the AlInP/GaInP structure coated with the DLAR coating and the four-layer ARC over the AlInP/GaInP structure without AR coating (labeled as "no ARC" in Figure 4a). It is particularly interesting to note that for $\theta \geq 50°$, the four-layer ARC has a substantially better performance than the DLAR coating. From Figure 4b, the averaged calculated transmittance improvement for $\theta = 50°$–80° is 18% for DLAR coating and 38% for four-layer ARC. As compared to the uncoated and DLAR coating IMM solar cells, the lower reflectance of the four-layer ARC is visually evident from the photograph of Figure 1b, which shows text reflected off the surface of each of the three devices.

Experimentally demonstrating the superior omnidirectional photovoltaic performance of four-layer ARC compared to DLAR coating, we studied two IMM solar cells, labeled IMM_1 and IMM_2, employing DLAR coating and four-layer ARC, respectively. Both IMM_1 and IMM_2 solar cell devices were characterized by an AOI-dependent current versus voltage measurement setup before and after AR coating deposition. The light source used in this setup is a 150 W xenon arc lamp and the light beam was attenuated by an AM0 filter. The current-density versus voltage (J–V) characteristics were measured for $\theta = 0°$–80° with 5° spacings. The J–V measurements were found to be repeatable, having less than 1% deviation for two separate J–V characterizations of each IMM solar cell device. The raw J–V performances of the DLAR coating and four-layer ARC coated IMM devices (see Figure S4, Supporting Information) were normalized to the corresponding short-circuit current density J_{SC} of uncoated IMM solar cells, and then compared.

Figure 5 summarizes the normalized measured J–V characteristics of IMM_1 and IMM_2 before and after AR coating deposition at two different illumination AOIs (0° and 80°). The measured J_{SC} improvements at normal incidence are 27.5% for DLAR coating on IMM_1 and 31.6% for the four-layer ARC on IMM_2, showing an excellent agreement with the anticipated improvement obtained from calculations. The measured J_{SC} improvement of the four-layer ARC is even more pronounced than that of DLAR coating at $\theta = 80°$, where the gain in J_{SC} for the DLAR coating worsens to 5.3% while that for the four-layer ARC improves to 53.3%.

To gauge the impact of the DLAR coating and four-layer ARC on the maximum power output, P_{max}, of the IMM devices, the P_{max} and the fill factor (FF) are extracted from J–V curves of the IMM_1 and IMM_2 devices, before and after AR coating deposition (see Figure S4, Supporting Information), and summarized in **Table 2**. The enhancement of maximum power output P_{max} due to the four-layer ARC is better than the corresponding enhancement due to the DLAR coating at normal incidence, where the DLAR coating improves the P_{max} by 28.9%, and the four-layer ARC improves the P_{max} by 34.2%. Further, the enhancement of P_{max} of four-layer ARC is significantly better than that of DLAR coating at strongly oblique AOIs: For example, at an AOI of 80°, the DLAR coating improves the P_{max} by only 4.9% but the four-layer ARC improves the P_{max} by 55.8%. Reading from the FF column, the DLAR coating and the four-layer ARC generally have no impact on the FFs of the IMM solar cells.

Lastly, to show a complete evaluation of omnidirectional photovoltaic performance of IMM solar cells with DLAR coating and four-layer ARC, we plot the ratio of J_{SC} measured after AR coating deposition to the J_{SC} measured before AR coating deposition. **Figure 6** shows the measured improvements in J_{SC} as a function of AOI for DLAR coating and four-layer ARC. The figure clearly shows that the IMM device utilizing the four-layer

© 2013 WILEY-VCH Verlag GmbH & Co. KGaA, Weinheim

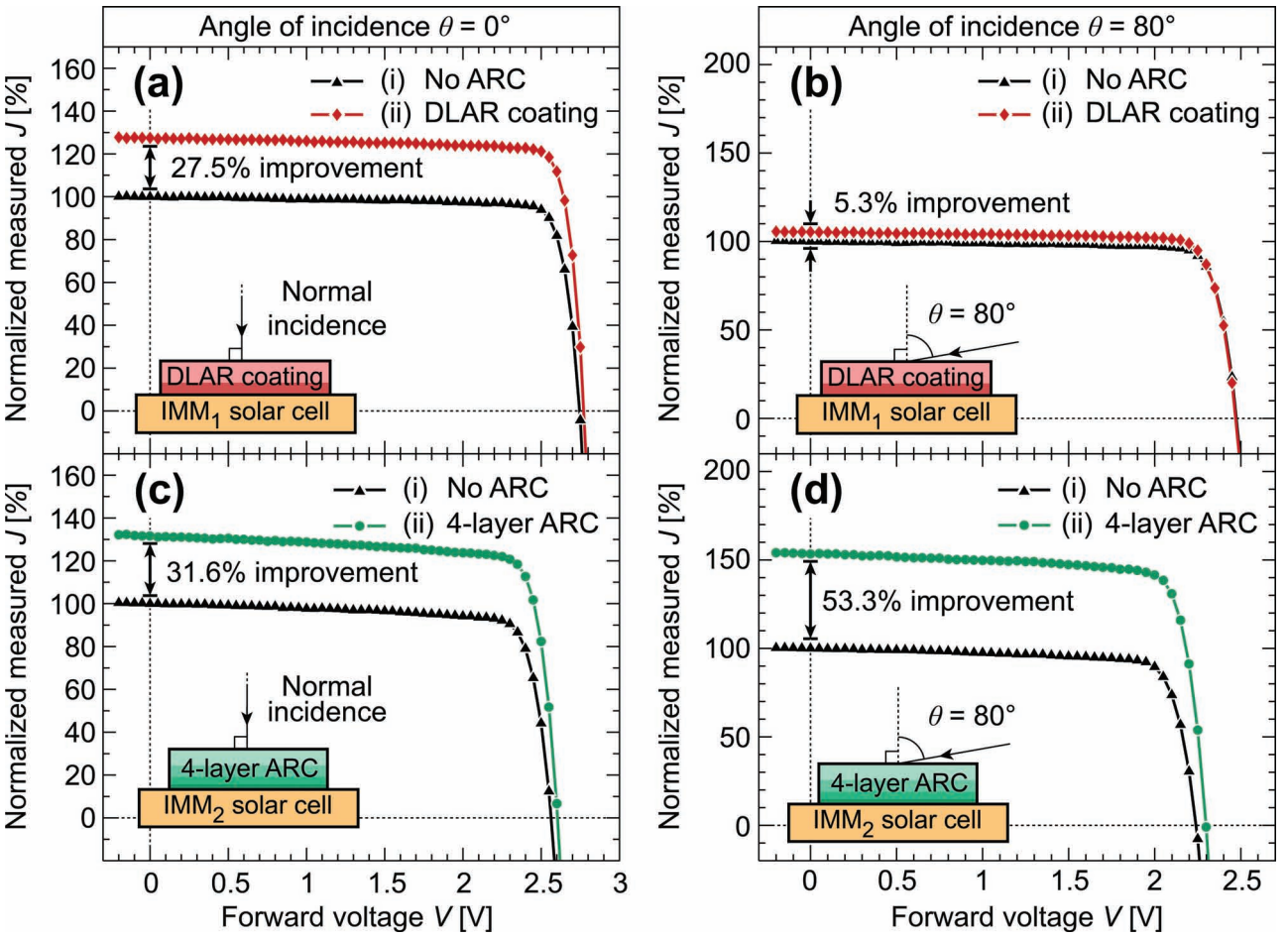

Figure 5. Measured current-density versus voltage (*J–V*) characteristics for IMM devices (i) without and (ii) with AR coating. Figure 5a–d shows (a) DLAR coating at normal incidence, (b) DLAR coating at AOI of 80°, (c) four-layer ARC at normal incidence and (d) four-layer ARC at AOI of 80°. All current density values are normalized to the J_{SC} value measured on the corresponding IMM devices before AR coating deposition. The illumination source is a 150 W xenon arc lamp attenuated by an AM0 filter. Devices were maintained at 27 °C during *J–V* characterization. The raw dark *J–V* data after AR coating deposition, and the raw light *J–V* data before and after AR coating deposition for IMM_1 and IMM_2 devices can be found in Figure S4, Supporting Information.

Table 2. Short-circuit current density (J_{SC}), open circuit voltage (V_{OC}), fill factor (*FF*) and maximum output power (P_{max}) of IMM_1 and IMM_2 triple-junction solar cells, without and with AR coating, at normal incidence and at AOI of 80°. The IMM devices were under illumination of an AM0 filter-attenuated 150 W xenon arc lamp, and maintained at 27 °C during *J–V* characterization. Also shown in this table are the P_{max} enhancements by the DLAR coating on IMM_1 and by the four-layer ARC on IMM_2.[a)]

	J_{SC} [mA cm^{-2}]	V_{OC} [V]	*FF*	P_{max} [mW]	P_{max} enhancement [%]
AOI θ = 0° (normal incidence)					
IMM_1: No ARC	4.67	2.75	0.86	12.8	–
IMM_1: DLAR coating	5.95	2.77	0.86	16.5	28.9
IMM_2: No ARC	4.46	2.56	0.81	11.4	–
IMM_2: Four-layer ARC	5.88	2.61	0.81	15.3	34.2
AOI θ = 80°					
IMM_1: No ARC	0.49	2.47	0.85	1.02	–
IMM_1: DLAR coating	0.52	2.47	0.84	1.07	4.9
IMM_2: No ARC	0.48	2.24	0.80	0.86	–
IMM_2: Four-layer ARC	0.73	2.30	0.80	1.34	55.8

[a)]The V_{OC} values are linearly interpolated from *J–V* curves at $J = 0$.

© 2013 WILEY-VCH Verlag GmbH & Co. KGaA, Weinheim

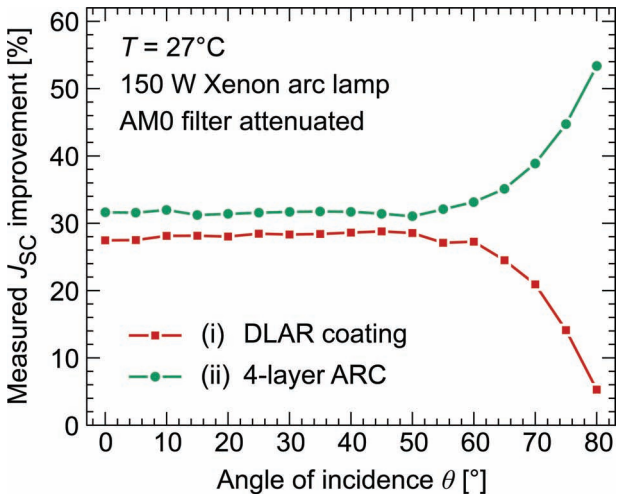

Figure 6. Measured J_{SC} improvement as a function of AOI for (i) IMM_1 device with DLAR coating and (ii) IMM_2 device with four-layer ARC. J_{SC} improvements are obtained as the ratio of the measured J_{SC} on IMM solar cells after AR coating deposition to that before AR coating deposition.

ARC outperforms the IMM device with traditional DLAR coating at all AOIs. The averaged improvements to J_{SC} over $\theta = 0°–80°$ is 25.3% for DLAR coating and 34.4% for four-layer ARC. Considering the effective area of the solar cell under illumination from different incident angles, the $\cos(\theta)$ weighted average J_{SC} improvement over $\theta = 0°–80°$ are 27.1% for IMM device with DLAR coating and 32.6% for IMM device with four-layer ARC.

IMM device with four-layer ARC shows particularly better photovoltaic performance at large AOIs (50°–80°) where DLAR coating becomes drastically ineffective. The averaged improvement in J_{SC} over $\theta = 50°–80°$ is 21.1% for DLAR coating, whereas the improvement to J_{SC} with the same averaging range for four-layer ARC yields 38.3%. The measured J_{SC} improvements agree well with the calculated transmittance improvement shown in Figure 4b for both IMM devices with DLAR coating and four-layer ARC. As a result, we demonstrate not only that the four-layer ARC shows better broadband and omnidirectional AR characteristics, but also that these exceptional AR characteristics of the four-layer ARC result in the expected photovoltaic performance enhancement when applied to the IMM solar cells.

3. Conclusions

We have demonstrated a GA-optimized four-layer discrete-refractive-index AR coating made of nanoporous tailored- and low-refractive index SiO_2 and co-sputtered SiO_2/TiO_2 on IMM solar cells devices. This four-layer ARC significantly outperforms the conventional DLAR coating over a wide range of AOIs (0–80°), achieving an averaged J_{SC} improvement of 34.4%. We attribute the excellent performance of this discrete-refractive index four-layer ARC to an excellent refractive index matching to the air ambient owing to low-refractive index nanoporous materials as well as optimized interference effects by a global optimization algorithm, i.e., the GA used here. Because the fabrication process of the four-layer ARC is additive and purely physical, it is fully compatible with the current manufacturing process of multijunction solar cells. Additionally, the tailorability and optimization of such a customizable approach readily lends itself to the incorporation of the AR coating design into solar cell device structures for application-specific requirements. Therefore, this four-layer ARC, as an example of the potential multiple-discrete-layer tailored- and low-refractive index AR coating technology, is viable, readily applicable and highly promising for future generations of AR coating technology on solar cell devices.

4. Experimental Section

Fabrication: Diced 1 cm × 1 cm IMM solar cell devices provided by MicroLink Devices Inc.[36] were detached from a silicon holding wafer. The back contact of the IMM device was then attached to a gold contact on the surface of a glass slide using conducting epoxy. The conducting epoxy was hardened in a standard laboratory oven at 150 °C for 60 min. After curing (hardening), the top contact of the IMM device was connected to a separate gold contact on the glass slide using a wire bonder. Examples of the finished device fixtures are shown in Figure 1b. Both the DLAR coating and four-layer ARC structure were globally optimized utilizing a computational genetic algorithm. The exact details of the optimization process are given in the Supporting Information. The DLAR coating was fabricated by RF magnetron sputtering. The first layer was deposited by RF sputtering of TiO_2; the second layer was deposited by RF sputtering of SiO_2. In each deposition, the RF power of the target was 200 W; the O_2 flow rate was 0.5 sccm, the Ar flow rate was 10 sccm. The chamber pressure was kept at 2 mTorr during sputtering deposition. The four-layer ARC was fabricated by RF co-sputtering of tailored-refractive index dense layers (Layer-1 and Layer-2) followed by oblique-angle e-beam deposition of tailored- and low-refractive index nanoporous layers (Layer-3 and Layer-4). Layer-1 was fabricated by RF sputtering of a TiO_2 target with a RF power of 200 W; the deposition rate for Layer-1 was 1.2 nm min^{-1}. Layer-2 was fabricated by RF co-sputtering of SiO_2 and TiO_2 with TiO_2 RF power of 200 W and SiO_2 RF power of 115 W; the deposition rate of Layer-2 was 3.3 nm min^{-1}. The O_2 flow rate, Ar flow rate and chamber pressure were as the same as the conditions used for DLAR coating deposition. For Layer-3 deposition, the solar cell was rotated to have a fixed deposition angle of 57° between the solar cell substrate normal and the SiO_2 vapor flux direction to achieve a porosity of 26%. For Layer-4 deposition, the solar cell substrate was rotated to have a fixed deposition angle of 85° between the solar cell substrate normal and the SiO_2 vapor flux direction to achieve a porosity of 80%. For uniform nanostructure morphology, the e-beam deposition rates of SiO_2 for Layer-3 and Layer-4 were maintained at 0.2–0.3 nm s^{-1} as monitored by a quartz crystal sensor.

Characterization: The layer information, including refractive index and thickness, was measured by variable angle spectroscopic ellipsometry using a WVASE32 ellipsometer. The normal incidence reflectance of the solar cells was characterized by a JASCO-V570 (UV-VIS-NIR) spectrometer for the wavelength range 350–850 nm, and by a Nicolet 8700 FT-IR spectrometer (Thermo Electron Corporation) for wavelength range 850–1600 nm. The light source used in the AOI-dependent *J–V* characterization setup is an Oriel 150 W xenon arc lamp. The light spectrum emitted from the xenon lamp is attenuated by an AM0 filter, guided by a solid fiber bundle with numerical aperture N.A. = 0.56, and collimated by a Newport 76601 light guide collimating probe before incident on the surface of the solar cell device. The xenon lamp is turned on 75 min before each measurement to enter a stable thermal and illumination condition. A Newport 2931-C power meter is used to monitor the light output power of the xenon lamp before each *J–V* measurement. The solar cell sample is mounted on an *x-y* stage during photocurrent measurement. In order to eliminate the photocurrent

© 2013 WILEY-VCH Verlag GmbH & Co. KGaA, Weinheim

variation caused by beam uniformity, the solar cell device is aligned in both *x* and *y* direction. The temperature of the *x-y* stage is regulated to 27 °C using a temperature controller with active heating and passive room temperature cooling. The *J–V* characteristic is obtained using a Keithley 2400 multimeter in four-wire sensing mode to eliminate a resistance contribution from the probe and contact resistance.

Supporting Information

Supporting Information is available from the Wiley Online Library or from the author.

Acknowledgements

The authors thank J. A. Bur, V. C. Elarde (MicroLink Devices Inc.), S.-Y. Lin, and F. W. Mont for useful discussions. The authors acknowledge support by Samsung Electronics Co., Korean Ministry of Knowledge Economy and Korea Institute for Advancement of Technology through International Collaborative R&D Program, the National Science Foundation, Sandia National Laboratories, Department of Energy, the National Research Foundation of Korea Grant funded by the Korean Government (MEST) (NRF-2011-220-D00064), Raydex Technology, Inc., and the United States Air Force.

Received: April 13, 2012
Revised: June 14, 2012
Published online: September 17, 2012

[1] M. A. Green, K. Emery, Y. Hishikawa, W. Warta, E. D. Dunlop, *Prog. Photovoltaics* **2012**, *20*, 12–20.
[2] J. Geisz, D. Friedman, J. Ward, A. Duda, W. Olavarria, T. Moriarty, J. Kiehl, M. Romero, A. Norman, K. Jones, *Appl. Phys. Lett.* **2008**, *93*, 123505.
[3] J. Zhao, A. Wang, P. Altermatt, M. Green *Appl. Phys. Lett.* **1995**, *66*, 3636–3638.
[4] S. Lee, S. Choi, J. Yi, *Thin Solid Films* **2000**, *376*, 208–213.
[5] P. Doshi, G. E. Jellison, A. Rohatgi, *Appl. Opt.* **1997**, *36*, 7826–7837.
[6] M. Cid, N. Stem, C. Brunetti, A. Beloto, C. Ramos, *Surf. Coat. Technol.* **1998**, *106*, 117–120.
[7] B. Richards, *Sol. Energy Mater. Sol. Cells* **2003**, *79*, 369–390.
[8] J. Nelson, *The Physics of Solar Cells*, Imperial College, London, UK **2003**, pp. 21–23.
[9] R. Winston, J. C. Miñano, P. Benítez, *Nonimaging Optics*, Elsevier Academic Press, USA **2005**, pp. 26–27.
[10] M. Victoria, C. Domínguez, I. Antón, G. Sala, *Opt. Express* **2012**, *20*, 8136–8147.
[11] S. Walheim, E. Schäffer, J. Mlynek, U. Steiner, *Science* **1999**, *283*, 520–522.
[12] N. F. Wang, T. W. Kuo, Y. Z. Tsai, S. X. Lin, P. K. Hung, C. L. Lin, M. P. Houng, *Opt. Express* **2012**, *20*, 7445–7453.
[13] Y. F. Huang, S. Chattopadhyay, Y. J. Jen, C. Y. Peng, T. A. Liu, Y. K. Hsu, C. L. Pan, H. C. Lo, C. H. Hsu, Y. H. Chang, *Nat. Nanotechnol.* **2007**, *2*, 770–774.
[14] J. W. Leem, J. S. Yu, Y. M. Song, Y. T. Lee, *Sol. Energy Mater. Sol. Cells* **2011**, *95*, 669–676.
[15] Q. Chen, G. Hubbard, P. A. Shields, C. Liu, D. W. E. Allsopp, W. N. Wang, S. Abbott, *Appl. Phys. Lett.* **2009**, *94*, 263118.
[16] J. Tommila, V. Polojärvi, A. Aho, A. Tukiainen, J. Viheriälä, J. Salmi, A. Schramm, JM Kontio, A. Turtiainen, T. Niemi, *Sol. Energy Mater. Sol. Cells* **2010**, *94*, 1845–1848.
[17] Y. J. Lee, D. S. Ruby, D. W. Peters, B. B. McKenzie, J. W. P. Hsu, *Nano Lett.* **2008**, *8*, 1501–1505.
[18] S. L. Diedenhofen, G. Grzela, E. Haverkamp, G. Bauhuis, J. Schermer, J. G. Rivas, *Sol. Energy Mater. Sol. Cells* **2012**, *101*, 308–314.
[19] J. W. S. Rayleigh, *Proc. London Math. Soc.* **1880**, *11*, 51–56.
[20] J. Q. Xi, J. K. Kim, E. F. Schubert, *Nano Lett.* **2005**, *5*, 1385–1387.
[21] J. Q. Xi, M. F. Schubert, J. K. Kim, E. F. Schubert, M. Chen, S. Y. Lin, W. Liu, J. A. Smart, *Nat. Photonics* **2007**, *1*, 176–179.
[22] J. Q. Xi, M. Ojha, W. Cho, J. Plawsky, W. Gill, T. Gessmann, E. Schubert, *Opt. Lett.* **2005**, *30*, 1518–1520.
[23] J. K. Kim, T. Gessmann, E. F. Schubert, J. Q. Xi, H. Luo, J. Cho, C. Sone, Y. Park, *Appl. Phys. Lett.* **2006**, *88*, 013501.
[24] M. L. Kuo, D. J. Poxson, Y. S. Kim, F. W. Mont, J. K. Kim, E. F. Schubert, S. Y. Lin, *Opt. Lett.* **2008**, *33*, 2527–2529.
[25] J. K. Kim, S. Chhajed, M. F. Schubert, E. F. Schubert, A. J. Fischer, M. H. Crawford, J. Cho, H. Kim, C. Sone, *Adv. Mater.* **2008**, *20*, 801–804.
[26] C. Chang, P. Yu, C. Yang, *Appl. Phys. Lett.* **2009**, *94*, 051114.
[27] P. Yu, C. H. Chang, C. H. Chiu, C. S. Yang, J. C. Yu, H. C. Kuo, S. H. Hsu, Y. C. Chang, *Adv. Mater.* **2009**, *21*, 1618–1621.
[28] M. F. Schubert, J. Q. Xi, J. K. Kim, E. F. Schubert, *Appl. Phys. Lett.* **2007**, *90*, 141115.
[29] D. J. Poxson, F. W. Mont, M. F. Schubert, J. K. Kim, J. Cho, E. F. Schubert, *Opt. Express* **2010**, *18*, A594–A599.
[30] X. Yan, F. W. Mont, D. J. Poxson, J. Cho, E. F. Schubert, M. H. Kim, C. Sone, *J. Appl. Phys.* **2011**, *109*, 103113.
[31] W. Southwell, *Opt. Lett.* **1983**, *8*, 584–586.
[32] M. F. Schubert, F. W. Mont, S. Chhajed, D. J. Poxson, J. K. Kim, E. F. Schubert, *Opt. Express* **2008**, *16*, 5290–5298.
[33] M. F. Schubert, D. J. Poxson, F. W. Mont, J. K. Kim, E. F. Schubert, *Appl. Phys. Express* **2010**, *3*, 082502.
[34] D. J. Poxson, M. F. Schubert, F. W. Mont, E. Schubert, J. K. Kim, *Opt. Lett.* **2009**, *34*, 728–730.
[35] S. Chhajed, D. J. Poxson, X. Yan, J. Cho, E. F. Schubert, R. E. Welser, A. K. Sood, J. K. Kim, *Appl. Phys. Express* **2011**, *4*, 052503.
[36] R. Tatavarti, A. Wibowo, G. Martin, F. Tuminello, C. Youtsey, G. Hillier, N. Pan, M. Wanlass, M. Romero, Proceedings of IEEE 35th Photovoltaic Specialist Conference, **2010**, 002125.
[37] D. J. Poxson, F. W. Mont, M. F. Schubert, J. K. Kim, E. F. Schubert, *Appl. Phys. Lett.* **2008**, *93*, 101914.

© 2013 WILEY-VCH Verlag GmbH & Co. KGaA, Weinheim